Journal of Ceramic Processing Research. Vol. 13, No. 4, pp. 398~404 (2012)

J O U R N A L O F
Ceramic Processing Research

Self assembly of biomimetic hydroxyapatite on the surface of different polymer thin films

M. Petrović[a], B. Čolović[b], V. Jokanović[b,*] and Dejan Marković[c]

[a]*Clinic for Maxillofacial Surgery, Faculty of Dentistry, Dr Subotića 4, Belgrade, Serbia*

[b]*Institute of Nuclear Sciences "Vinča", Laboratory of Radiation Chemistry and Physics, Mike Petrovića Alasa 12-14, Vinča, University of Belgrade, Serbia*

[c]*Faculty of Dentistry, Belgrade University, Dr Subotića 4, Belgrade, Serbia*

The role of the process of designing a scaffold in bone tissue engineering is to provide optimal conditions for new bone tissue growth. The primary concern of such engineering is to create an adequate nanotopology of the scaffold inner walls, which can initiate the growth and activity of bone cells. Here, we present a completely new scaffold designing process based on a biomimetic approach in order to improve the nanostructure of pore walls of previously-made calcium hydroxyapatite (CHA) porous scaffolds. CHA porous scaffolds were covered with different polymer thin films (alginate, cellulose and PLGA) and exposed to simulated body fluid (SBF) for 42 days. SBF induced in situ formation of "bone-like" apatite phases on the surface of CHA/polymer composites. Fourier Transformed Infrared (FTIR) spectroscopy showed that the biomimetically-assembled phase is CHA of slightly shifted stoichiometry. X-ray diffraction confirmed that CHA is self-assembled on the surface of all investigated thin films. The calculation of crystallite sizes showed small differences in the degree of crystallinity between different samples. Scanning electron microscopy revealed a dominant blow-ball morphology of CHA particles (size 1 - 5 μm) with nano-sized branches on their surfaces.

Key words: Self assembling, Biomimetic, Bioactive thin films, Hydroxyapatite, Nanotopology design.

Introduction

The principles of bone tissue engineering are based on the construction of active, porous ceramic structures, known as scaffolds, of a well-defined inner wall morphology. These structures are mostly made of calcium hydroxyapatite (CHA) of slightly shifted stoichiometry. CHA scaffolds have been widely tested in dentistry and orthopedic surgery due to their biocompatibility and osteoconductivity [1, 2]. Because its architecture is similar to those of real bones, porous CHA is being used as a filling material for bone defects and in prosthesis revision surgery [3]. When combined with appropriate polymer/ biopolymer thin films (because of their biocompatibility, mechanical properties and biodegradability), scaffolds can provide a good basis for the initiation of the growth and activity of bone cells [4]. Besides scaffold porosity and its distribution, pore topology (the appearance of structural elements that form pore walls and their mutual arrangements) is also very important. Polymers applied in scaffold design improve the nanotopology of scaffold inner walls, and also, their incorporation into the scaffold structure enables further activation of the cells and facilitates the process of cell proliferation and growth. One of the most commonly used polymers in the last decade is PLGA (a copolymer of PLA-poly lactic acid and PGA-poly glycolic acid) because of its medically-approved status and degradation rate which may be controlled by manipulating the composition and ratio of the co-polymers [5-7]. Also, natural polysaccharides are promising materials for biomimetic mineralization of calcium phosphate-based ceramics on a nanoscale because of their supramolecular pre-organization by self-assembling of polysaccharide chains, formation of cellular templates with higher-order architectures, and site-selective nucleation of calcium phosphate at the biopolymer template surface. Thus, polysaccharide-based structural templates may serve to improve chemical and functional properties of different ceramic scaffold structures which is important for cell adhesion and growth [8]. Cellulose is one of the candidates among polysaccharides investigated for scaffold fabrication in bone tissue engineering due to its very good biocompatibility, and potentially it can be considered as an energy source for cells [9, 10]. Also, it is known to be slowly degradable with a degradation rate dependent on the chain length and degree of crystallinity, so it is possible to manipulate the rate of degradation [8]. Another natural polysaccharide, suitable for scaffold designing, is alginate. Sodium alginate has been used mainly for encapsulation and immobilization of a variety of cells and drugs but also it was shown to be efficacious when used in bone tissue engineering [11-15].

*Corresponding author:
Tel : +381-11-3408-724
Fax: +381-11- 3408-607
E-mail: vukoman@vinca.rs

Free cell growth requires 3-dimensional carriers with well defined structures, organized, at least, on two levels: first in the range of several dozens of micrometers and the second in the nano-range. The second level of structural organization includes proper design of scaffold surface topography. An appropriate morphology of scaffold walls can be achieved by using a specific nanodesign of hydroxyapatite particles inside the biomimetic medium, when they are self-assembled on the polymer/ceramic scaffold structure [16].

The subject of this paper is an improved design of a ceramic CHA scaffold obtained by using polyurethane foam template. For an advanced design of the scaffold nanotopology, the biomimetic method was applied because as shown in our previous investigations it can yield "bone-like" structures [17, 18]. To the best of our knowledge this is a new approach in scaffold design and can be used for the additional design of scaffolds obtained by applying any of the methods (sol-gel technique, thermally-induced phase separation, electrophoretic deposition, etc.). In this study, three different types of polymers (PLGA, cellulose and alginate) were used for the functionalisation of the inner walls of CHA scaffolds. The CHA/polymer composite is actually a new carrier of enhanced properties, serving to advance the nanotopology design of scaffold inner walls by a biomimetic treatment in a modified SBF medium. The *in vitro* structures obtained may be of great importance for improved nanostructure design of 3D scaffold inner walls, but also they mimic the possible development of such structures under *in vivo* conditions [19- 21].

Experimental procedure

Methods of preparation and materials

Porous CHA carrier/scaffolds, covered with thin polymer films (alginate, cellulose or PLGA), were used as substrates for CHA biomimetic deposition.

Porous CHA was prepared as follows. First, CHA powder was prepared hydrothermally, assisted with a surface active substance poly(ethylene vinyl acetate/ ethylene vinyl versatate) (EVA/EVV). CHA-EVA/EVV core shell composite powder was then dispersed in water and treated mechanochemically to redce the CHA grain sizes. When a uniform mass was achieved, the slip obtained was poured over polyurethane foam with the required pore size distribution. This system was pyrolysed in order to burn away the polyurethane template and sintered at 1300 °C for 3 h to obtain satisfactory mechanical properties of the porous CHA scaffold.

Thin films of alginate, cellulose and PLGA were then deposited (the alginate and cellulose were dissolved in water and PLGA in chloroform, in a concentration 1% w/ w) over scaffold samples. The thicknesses of the deposited polymer films were of the order of one micrometer.

The CHA porous carrier/scaffold was immersed in SBF prepared by a modified procedure (concentration (mol dm^{-3}) of each ion was: Cl^- - 0.054, Na^+ - 0.0542, Ca^{2+} - 0.0025, PO_4^{3-} - 0.001, Mg^{2+} - 0.0003, CO_3^{2-} - 0.0006 and K^+ - 0.0014; pH was adjusted at 7.4) and left to age for 6 weeks at 37 °C (in a universal oven, MEMMERT model UNB 400). The SBF was refreshed every 48 h. The pH was periodically controlled. After ageing, the samples were removed from the medium, rinsed with deionized water and characterized.

Characterization

The phases assembled on different polymer films were examined by a Fourier transform infrared spectrometer (Nicollet 380 FTIR, Thermo Electron Corporation) in the attenuated total reflectance (ATR) mode. FTIR spectra were recorded in the spectral range 4000-400 cm^{-1}.

An X-ray diffraction (XRD) method (Philips PW 1050) was used for phase analysis of the phases obtained. Data were analyzed in the range of 2θ from 9 to 67 ° with a scanning step of 5 °, and exposure time of 2 s per step. Crystallite sizes were calculated using the Scherrer equation, $d = K\lambda/B\cos\theta$, where d (in nm) is the average diameter of crystallites, K is the shape factor, B is the width of the (121) diffraction at the half of its maximum height, λ is the wavelength of the X rays used, and θ is the Brag diffraction angle.

Elemental analysis was done by an energy dispersive X ray spectrometer (QX 2000 – Oxford Instruments) combined with SEM and a multichannel analyzer in order to estimate the chemical homogeneity of the self-assembled CHA. The Ca/P ratio was determined using the ZAF (Link Company) software package.

Scanning electron microscopy (SEM) was used to investigate the sample morphology and microstructure. Samples were sputter coated with gold and observed using a JOEL SEM.

Results and discussion

CHA powder and scaffold structural and morphological properties

CHA powder, used for scaffold preparation, has a very fine structure. It consists of agglomerates (Fig. 1),

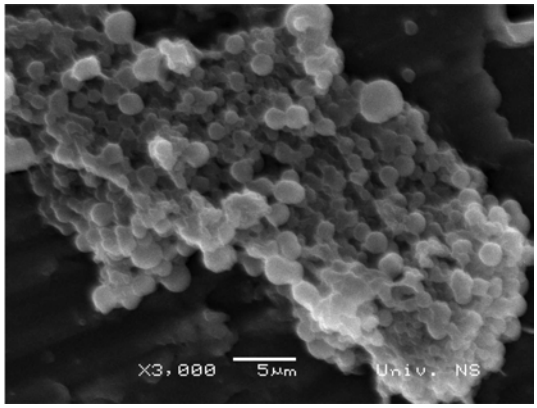

Fig. 1. SEM micrograph of the CHA powder.

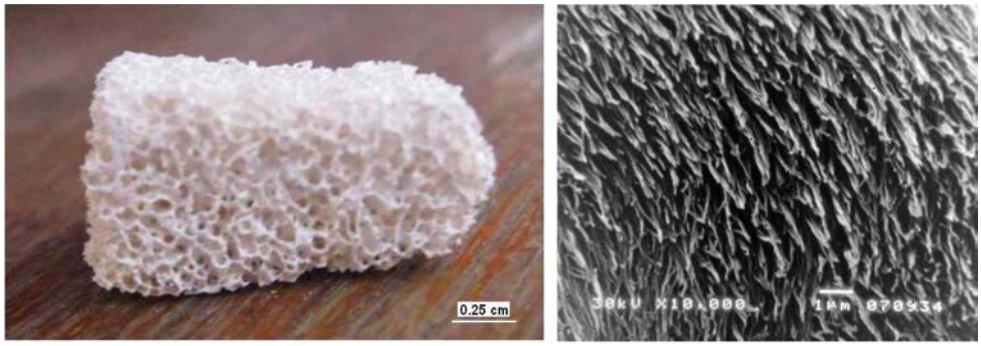

Fig. 2. CHA scaffold: a) photograph of a scaffold piece, b) SEM micrograph: the typical appearance of the scaffold walls

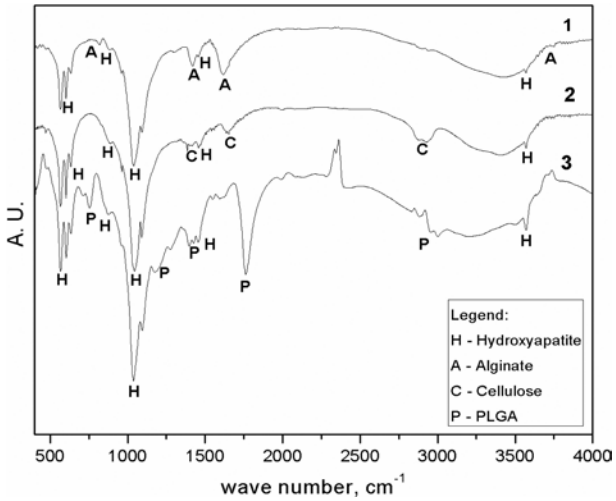

Fig. 3. IR spectra of CHA self assembled on different polymer films: 1–alginate, 2–cellulose, 3–PLGA

which are very similar in shape and size (1-5 μm) and are built up from fine particles 200 nm in size.

The CHA scaffold, synthesized from the hydroxyapatite powder has a highly porous 3D structure (Fig. 2a). Pores are cylindrical and interconnected with a width in the range of 0.1 to 1 mm, while the most numerous are those of a width 0.2 - 0.3 mm. Also, it has a very defined internal geometry- porosity, with pores of the order of 200 nm to 1 mm. On Fig. 2b the needle structure of the ceramic walls can be observed, with a length of needles of 1 μm and diameter of 50 nm.

FTIR analysis

Analysis of FTIR spectra reveal that the phase biomimetically assembled on the surface of CHA/polymer composites is CHA of slightly shifted stoichiometry.

All three IR spectra in Fig. 3. show the bands characteristic of CHA: a weak band corresponding to hydroxyl stretching is observed at about 3570 cm^{-1}; the bands at about 1640 cm^{-1} are assigned to the bending mode of OH^- groups; bands located at 600 to 650 cm^{-1} are ascribed to the liberation mode of the O-H vibration; asymmetric stretching vibration of PO_4^{3-} is found at about 970-1090 cm^{-1}; symmetric stretching vibrations of PO_4^{3-} are present at 550 to 640 cm^{-1}, while the bands at about 430 to 450 cm^{-1} correspond partially to the ν_2 symmetric mode of the PO_4^{3-} vibration; the bands corresponding to CO_3^{2-} are present at 1458 cm^{-1} (ν_{3b} of B type carbonated hydroxyapatite) and about 1420 cm^{-1} (ν_{3a} of B type carbonated hydroxyapatite); the presence of carbonate (CO_3^{2-}) is also indicated by the band around 870 cm^{-1} [17, 22, 23]. The fact that type B of carbonated hydroxyapatite is prevailing is very significant because this phase has the highest activity among carbonated hydroxyapatites (it prevails in young bones).

The bands characteristic of each polymer are also visible in the IR spectra:

Alginate: the bands present at about 3500-3700 cm^{-1} are assigned to the OH stretch; the bands at about 1615 and 1420 cm^{-1} correspond to the antisymmetric and symmetric stretching vibration of COO^-, respectively; the band observed at about 1640 cm^{-1} can be assigned to water associated with the biopolymer; skeletal vibrations are observed at around 1300 cm^{-1}; the bands corresponding to antisymmetric stretching of C-O-C at about 1080-1020 cm^{-1} are partially hidden by CHA bands; the bands present at about 820 cm^{-1} are identified in the literature as the combination of three possible vibrational modes: bending modes of - CCO and - CCH groups and twisting mode of C = O group [24-24].

Cellulose: the bands at 2920 and 2940 cm^{-1} correspond to C = O and C-H stretching vibrations, respectively; the band found at around 2900 cm^{-1} belongs to O-H stretch, while the O-H bending mode of adsorbed water is registered at about 1640 cm^{-1}; the band at around 1590 cm^{-1} confirms the presence of the COO^- group; the bands at about 1430 cm^{-1} are assigned to HCH and OCH in-plane bending vibrations and the band at about 1380 cm^{-1} corresponds to the C-H bending mode; the bands at around 900 cm^{-1} are attributed to the COC, CCO and CCH deformation modes and stretching vibrations corresponding to the motions of C-5 and C-6 atoms; the C-OH out-of-plane

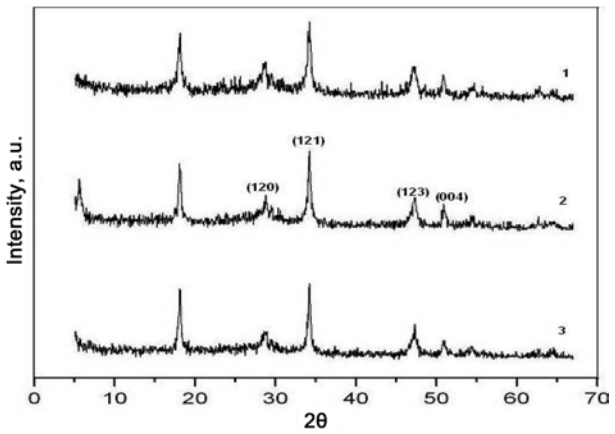

Fig. 4. XRD spectra of CHA self assembled on different polymer films: 1−alginate, 2−cellulose, 3− PLGA

bending mode is supposed to be at about 670 cm^{-1} but it is hidden by the bands corresponding to CHA [27-30].

PLGA: the band registered at 2995 cm^{-1} corresponds to the C-H asymmetric stretching vibration, while the bands at around 2950 and 2880 cm^{-1} correspond to the C-H symmetric stretch; a strong band at 1760 cm^{-1} is attributed to the C = O stretch; the bands at about 1100-1280 cm^{-1} are ascribed to the aliphatic ether C-O-C stretch; the bands found in the region 1400-1500 cm^{-1} correspond to CH_2, CH_3, and CH deformation vibrations; and the band registered at around 750 cm^{-1} is assigned to the rocking motion of long CH_2 chains [30-32].

XRD and EDS analysis

The characteristic diffraction peaks corresponding to (121), (120), (123) and (004) plane show clearly that CHA is self-assembled on the surface of all the thin films investigated (cellulose, alginate and PLGA) deposed on the surface of CHA scaffolds (Fig. 4). The calculation of crystallite sizes, using the Scherrer formula, showed small differences in the degree of crystallinity between different samples (average crystallite sizes were: for cellulose 19.7 nm, alginate 21.7 nm and PLGA 24.1 nm). Although the smallest values of the crystallite sizes were obtained for the CHA self-assembled on the surface of the cellulose thin film and the largest value for the PLGA thin film, these differences are negligible.

Besides, semi-quantitative chemical analysis assessed by EDS showed that values of Ca/P ratio, for all thin films, are similar to values for stoichiometric CHA (for cellulose 1.58, alginate 1.62 and PLGA 1.65).

SEM analysis

The SEM study revealed a very well-developed morphology of CHA particles.

As can be seen in Fig. 5, CHA assembled on the alginate thin film has different particle morphologies – blow-ball and polygonal shape. The particles of a polygonal shape are smaller; the diameter of the

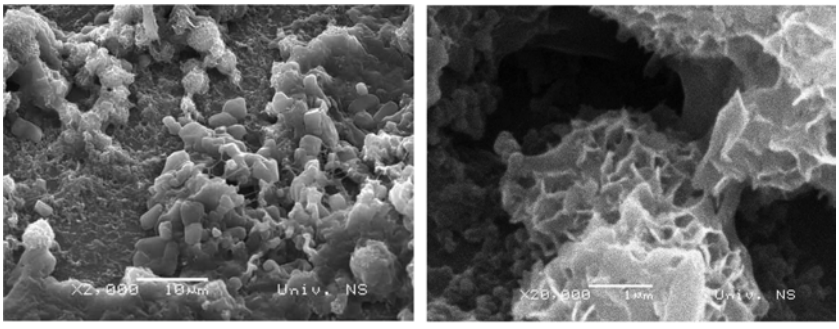

Fig. 5. CHA assembled on an alginate thin film: a) lower magnification b) higher magnification

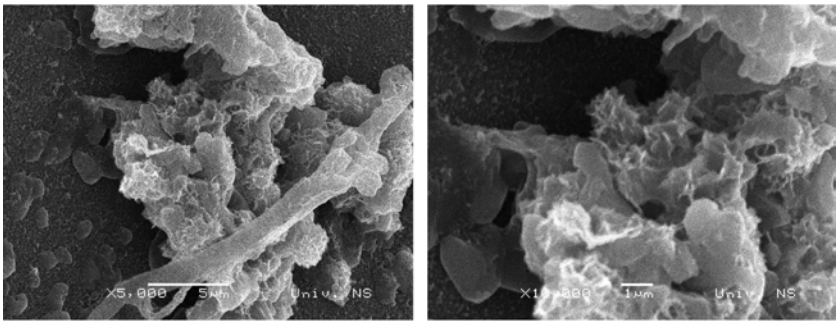

Fig. 6. CHA assembled on a cellulose thin film: a) lower magnification b) higher magnification

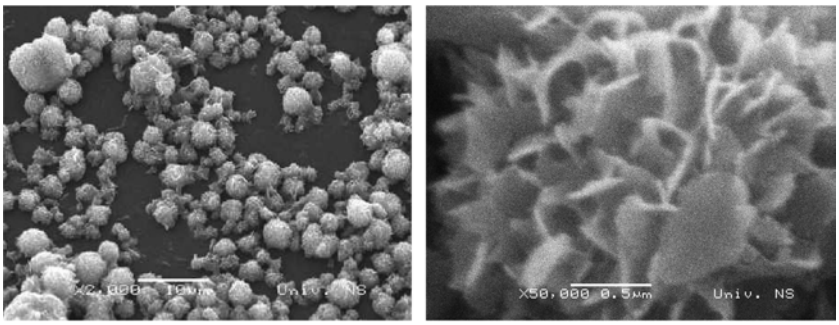

Fig. 7. CHA assembled on a PLGA thin film: a) lower magnification b) higher magnification

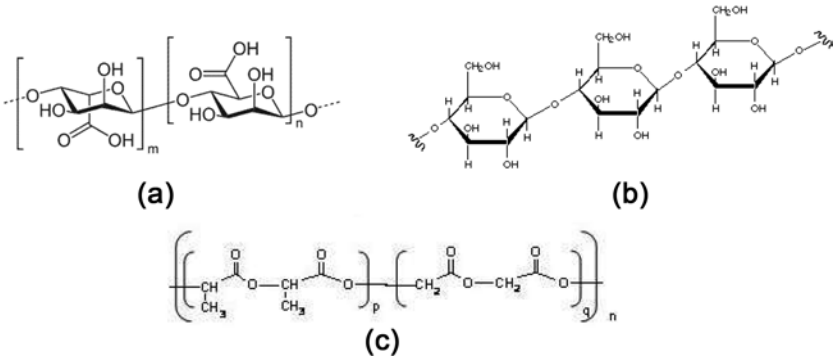

Fig. 8. Structural formula of: a) alginate, b) cellulose, c) PLGA

smallest particles is about 1 μm, while that of the largest ones is about 5 μm. The size distribution of blow-ball shaped particles is from 3 to 5 μm. The width of needle- like patterns on the surface of blow-ball particles is 18-25 nm, while the distance between them is in the range 150-500 μm.

Lee et al. [11] in a similar study observed a plate-like morphology of nucleated apatite with a particle size distribution in the range of 10-60 μm and a mean diameter of 27 μm. Some other authors [33, 34] also investigated apatite formation on alginate substrates, but did not observe such a well-developed particle morphology.

Fig. 6. shows the particle morphology of CHA assembled on a cellulose thin film-particles of irregular shapes with a very well-developed surface morphology. The mean diameter of most of the particles is about 3 μm and of the smallest ones about 1 μm. Needle-like and plate-like patterns are observed on the particle surface and the width of surface patterns is from 30 to 150 nm.

Nge et al. [35] obtained similar values of particle diameters (about 3 μm). They observed island-like hemispherical globules on the surface of bacterial cellulose microfibrils network after soaking in 1.5 SBF for 21 days. While investigating CHA self nucleation on cellulose, Wan et al. [36], observed spherical CHA particles that covered the entire surface of the substrate and also spaces among the fibers. At higher magnification, it can be seen that the spheres are composed of needle-like CHA crystals. The needle-like and plate-like shape morphologies were also observed by other authors [8, 9, 37, 38].

CHA self-assembled on the surface of a PLGA thin film is shown in Fig. 7: blow-ball shaped particles are observed exhibiting a highly developed morphology with petal like structures on the particle surfaces. The particle size is mostly in the range from 2.5 to 3.5 μm, but also there are some smaller particles (0.7-1.5 μm) and a small number of large once (4.3-8.5 μm). The width of petal-like structures on the particle surface is only 15-20 nm. The distance between the particles is in the range from 900 nm to 1.8 μm.

Similar values of particle sizes (mean particle diameter of 2.44 μm) were reported in a study dealing with apatite formation on PLGA scaffolds [39]. The particle morphology seems to be very similar to the morphology obtained in our study, but it cannot be clearly seen because of the low magnification. However, the number of particles on porous PLGA walls in contrast to what we have found is much lower, even when 1.5×SBF was used, but the nucleation time was shorter. Que et al. [40] also used 1.5×SBF for apatite nucleation on PLGA and the particle size was under half a micrometer for a nucleation time of 24 h.

Discussion

Understanding the mechanism of nucleation of

biomimetic CHA in SBF is important for advanced research in this field. Further improvements can be achieved by choosing adequate polymers for the scaffold functionalisation. As is well known, carboxyl/ hydroxyl groups in alginate, cellulose and PLGA chains act as active sites initiating nucleation (alginate has both carboxyl and hydroxyl groups, while cellulose and PLGA possess only hydroxyl and carboxyl groups, respectively, Fig. 8). These negatively charged groups, in the initial stage of nucleation, attract Ca^{2+} ions from the SBF which then become attached onto the polymer surfaces.

In the next step, PO_4^{3-} ions are attracted by positively charged Ca^{2+} ions. Therefore, the process of nucleation of calcium phosphate occurs by the initial attachment of Ca^{2+} ions onto the active sites of the corresponding polymers and subsequent attachment of PO_4^{3-} ions to Ca^{2+} ions. As already shown [8, 18, 35], the concentration of carboxyl/hydroxyl groups on the surface of polymer scaffolds (over the density of nucleation sites) probably plays a very important role in the rate and mechanism of calcium phosphate nucleation [41]. The density of nucleation sites may also affect the size of agglomerates and their morphology. The results given in this paper clearly confirm this assumption. The highest density of nucleated particles was observed in the case when the alginate was used, as shown in Fig. 5a. This was probably caused by the very high density of carboxyl and/or hydroxyl active groups present in alginate chains. However, in the case of PLGA, as is shown in Fig. 7a, a relatively low density of self-assembled particles was observed, probably due to significantly lower density of carboxyl active groups in the PLGA than in the alginate. Regarding the spatial arrangement of active hydroxyl groups in cellulose chains, it seems that they are relatively close to each other. Therefore, agglomerates from neighboring nucleation sites probably merged with each other causing the formation of elongated structures, as shown in Fig.6a. Accordingly, in samples where alginate and cellulose were used as substrate coatings, smaller particles were obtained (1-5 μm). This can be a result of the increased number of nucleation sites. Bigger agglomerates (some of them over 8 μm) were observed when PLGA was used, which probably has the smallest number of nucleation sites that further cause the corresponding growth of calcium phosphate nuclei and grains.

Self-assembled nanostructures obtained biomimetically in this study may play a significant role in cell growth on scaffold surfaces. Results obtained by the FTIR analysis (Fig. 3). show that the nucleated phase is the carbonated apatite, prevailing type B, which is present in biological systems, support this assumption. Several studies dealing with cell behavior on apatite formed on polymer surfaces confirmed its ability to favor osteoblast-like cell growth and to maintain their osteoblastic functionality [7, 12, 13, 42]. Our further investigations will be focused on cell behavior on structures obtained as described in this paper.

Conclusions

A new method of scaffold fabrication was presented in this study. An improved nanostructural design of a previously made CHA scaffold was achieved by a biomimetic treatment in SBF. In order to improve the nucleation of the biomimetic apatite phase, alginate, cellulose and PLGA thin films were deposited onto the scaffold surface before immersion in SBF. The phase biomimetically nucleated in SBF, according to FTIR measurements, is carbonated calcium hydroxyapatite, with the B type prevailing. XRD analysis confirmed that the self-assembled phase is CHA with crystallite sizes about 20 μm. EDS analysis showed that values of the Ca/P ratio, for all thin films, are similar to values for stoichiometric CHA. SEM micrographs clearly show “bone-like” structures in all cases. Especially good example of these structures can be seen in the case of the PLGA substrate.

This study showed how to obtain “bone-like” structures by additional nanodesigning of porous CHA scaffolds by a biomimetic treatment. The structures obtained mimic the morphology of natural bone and are suitable for cell adhesion and growth, providing faster bone regeneration, as shown in some studies. This mechanism of apatite formation *in vitro* is probably similar to the mechanism of bone tissue formation *in vivo.* Thus, a scaffold nanodesigned in this way could provide conditions similar to physiological ones for cell growth and proliferation.

Acknowledgement

Financial support for this study was granted by the Ministry of Education and Science of the Republic of Serbia (project no. 172026).

References

1. M.P. Ginebra, T. Traykova, J.A. Planell, J. Control. Release 113 (2006) 102-110.
2. W.J.E.M. Habraken, J.G.C. Wolke, J.A. Jansen, Adv. Drug Delivery Rev 59 (2007) 234-248.
3. B. Palazzoa, M.C. Sidoti, N. Roveri, A. Tampieri, M. Sandri, L. Bertolazzi, F. Galbusera, G. Dubini, P. Vena, R. Contro, Mater. Sci. Eng., C 25 (2005) 207-213.
4. R. Zhang, P.X. Ma, Macromol. Biosci. 4 (2004) 100-111.
5. S.S. Kim, M.S. Park, O. Jeon, C.Y. Choi, B.S. Kim, Biomaterials 27 (2006) 1399-1409.
6. A.C. Jayasuriya, M. Assad, A.H. Jayatissa, N.A. Ebraheim, Surf. Coat. Technol. 200 (2006) 6336-6339.
7. M. Ngiam, S. Liao, A.J. Patil, Z. Cheng, C.K. Chan, S. Ramakrishna, Bone 45 (2009) 4-16.
8. I. Hofmann, L. Müller, P. Greil, F.A. Müller, Surf. Coat. Technol. 201 (2006) 2392-2398.
9. P. Cromme, C. Zollfrank, L. Müller, F.A. Müller, P. Greil,

Mater. Sci. Eng., C 27 (2007) 1-7.
10. J.C. Fricain, P.L. Granja, M.A. Barbosa, B. de Jeso, N. Barthe, C. Baquey, Biomaterials 23 (2002) 971-980.
11. M. Lee, W. Li, R.K. Siu, J. Whang, X. Zhang, C. Soo, K. Ting, B.M. Wu, Biomaterials 30 (2009) 6094-6101.
12. A. Tampieri, M. Sandri, E. Landi, G. Celotti, N. Roveri, M. Mattioli-Belmonte, L. Virgili, F. Gabbanelli, G. Biagini, Acta Biomaterialia 1 (2005) 343-351.
13. L. Wang, R.M. Shelton, P.R. Cooper, M. Lawson, J.T. Triffitt, J.E. Barralet, Biomaterials 24 (2003) 3475-3481.
14. Z. Li, H.R. Ramay, K.D. Hauch, D. Xiao, M. Zhang, Biomaterials 26 (2005) 3919-3928.
15. A. Tampieri, G. Celotti, E. Landi, From biomimetic apatites to biologically inspired composites, Anal. Bioanal. Chem. 381 (2005) 568-576.
16. T.i. Ķokubo, Acta mater. 46 (1998) 2519-2527.
17. B. Čolović, B. Todorović -Marković, Z. Marković, D. Marković, M. Plavšić and V. Jokanović, Surf. Eng. 26 (2010) 532-535.
18. B. Čolović, V. Jokanović, B. Todorović -Marković, Z. Marković, Journal of Optoelectronics and Advanced Materials, 11 (2009) 70-75.
19. T. Kokubo, H. Takadama, Biomaterials 27 (2006) 2907−2915.
20. A. C. Tas, Biomaterials 21 (2000) 1429-1438.
21. X. Chen, B. Lei, Y. Wang, N. Zhao, Journal of Non-Crystalline Solids 355 (2009) 791−796.
22. K. Shin, A.C. Jayasuriya, D.H. Kohn, Journal of Biomedical Materials Research 83 A (2007) 1076-1086.
23. R.Z. LeGeros, in "H.M. Myers (Eds.), Calcium Phosphates in Oral Biology and Medicine", (California: Karger, 1999) p 82.
24. C.C. Ribeiro, C.C. Barrias, M.A. Barbosa, Biomaterials 25 (2004) 4363−4373.
25. B. Dupuy, A. Arien, A.P. Minnot, Art Cells, Blood Subs. Immob. Biotech. 20 (1994) 71−82.
26. G. Lawrie, I. Keen, B. Drew, A. Chandler-Temple, L. Rintoul, P. Fredericks, L. Grøndahl, Biomacromolecules 8 (2007) 2533-2541.
27. R.G. Zhbankov, S.P. Firsov, D.K. Buslov, N.A. Nikonenko, M.K. Marchewka, H. Ratajczak, J. Mol. Struct. 614 (2002) 117−125.
28. M.A. Sherif, S. Keshk, Carbohydr. Polym. 74 (2008) 942-945.
29. S.Y. Oh, D.I. Yoo, Y. Shin, G. Seo, Carbohydr. Res. 340 (2005) 417-428.
30. M.V. Jose, V. Thomas, K.T. Johnson, D.R. Dean, E. Nyairo, Acta Biomaterialia 5 (2009) 305−315.
31. S.E. Petricca, K.G. Marra, P.N. Kumta, Acta Biomaterialia 2 (2006) 277−286.
32. H. Tai, C.E. Upton, L.J. White, R. Pini, G. Storti, M. Mazzotti, K.M. Shakesheff, S.M. Howdle, Polymer 51 (2010) 1425−1431.
33. T. Kokubo, M. Hanakawa, M. Kawashita, M. Minoda, T. Beppu, T. Miyamoto, T. Nakamura, J. Mater. Sci.: Mater. Med. 15 (2004) 1007-1012.
34. T. Kokubo, M. Hanakawa, M. Kawashita, M. Minoda, T. Beppu, T. Miyamoto, T. Nakamura, Journal of the Ceramic Society of Japan, 112 (2004) 363-367.
35. T. Nge, J. Sugiyama, J. Biomed. Mater. Res., Part A, DOI 10.1002/jbm.a
36. Y.Z. Wan, Y. Huang, C.D. Yuan, S. Raman, Y. Zhu, H.J. Jiang, F. He, C. Gao, Mater. Sci. Eng., C 27 (2007) 855−864.
37. K. Sato, T. Kogure, Y. Kumagai, J. Tanaka, J. Colloid Interface Sci. 240 (2001) 133−138.
38. A. Ebrahimpour, M. Johnsson, C.F. Richardson, G.H. Nancollas, J. Colloid Interface Sci. 159 (1993) 158.
39. R. Zhang, P.X. Ma, Macromol. Biosci. 4 (2004) 100−111.
40. X. Qu, W. Cui, F. Yang, C. Min, H. Shen, J. Bei, S. Wang, Biomaterials 28 (2007) 9-18.
41. M. Hashizume, H. Horii, J. Kikuchi, M. Kamitakahara, C. Ohtsuki, M. Tanihara, J. Mater. Sci.: Mate. Med. 21 (2010) 11−19.
42. M. Tommila, A. Jokilammi, P. Terho, T. Wilson, R. Penttinen, E. Ekholm, J. R. Soc. Interface 6 (2009) 873-880.